Interpreting SAXS Data Recorded On Cellulose Rich Pulps

Tomas Larsson (tomas.larsson@ri.se)
RISE Innventia AB
Jasna Stevanic-Srndovic
RISE Innventia AB
Stephan V. Roth
DESY: Deutsches Elektronen-Synchrotron
Daniel Söderberg
KTH: Kungliga Tekniska Hogskolan

Research Article

Keywords: SAXS, modelling, cellulose, CP/MAS 13C-NMR, FSP, Pulp

Posted Date: June 2nd, 2021

DOI: https://doi.org/10.21203/rs.3.rs-561202/v1

Version of Record: A version of this preprint was published at Cellulose on November 10th, 2021. See the published version at https://doi.org/10.1007/s10570-021-04291-x.

Abstract

A simulation method was developed for modelling SAXS data recorded on cellulose rich pulps. The modelling method is independent of the establishments of separate form factors and structure factors and was used to model SAXS data recorded on dense samples. An advantage of the modelling method was that it made it possible to connect experimental SAXS data to apparent average sizes of particles and cavities at different sample solid contents. Experimental SAXS data could be modelled as a superposition of a limited number of simulated intensity components and gave results in qualitative agreement with CP/MAS ^{13}C-NMR data recorded on the same samples. For the water swollen samples, results obtained by the SAXS modelling method and results obtained from CP/MAS ^{13}C-NMR measurements, agreed on the ranking of particle sizes in the different samples. The SAXS modelling method is dependent on simulations of autocorrelation functions. The time needed for simulations could be reduced by rescaling of simulated correlation functions, due to their independence of the choice of step size in real space. This way an autocorrelation function simulated for a specific sample could be used to generate SAXS intensity profiles corresponding to all length scales for that sample and used for efficient modelling of the experimental data recorded on that sample.

Background

Small Angle X-ray Scattering (SAXS) is a versatile technique that can be used to obtain quantitative measures of the nanostructure in cellulose containing samples (Jakob et al. 1994, Jakob et al. 1996, Fratzl 2003, Keckes et al. 2003, Penttilä et al. 2019) Water-based dispersions of cellulose nanofibrils (CNF) has been the target of some recently published studies illustrating the capacity of the SAXS technique; Håkansson et al. 2014, Su et al 2015, Geng et al. 2017, Mao et al. 2017, Rosén et al. 2018, Brett et al. 2020. CNF can be produced by chemical modification, typically by carboxymethylation (Pääkkö et al 2007) or by TEMPO oxidation (Saito et al 2007) followed by subsequent mechanical homogenization and has been studied by x-ray scattering (c.f. Geng et al. 2017, Rosén et al. 2018). An often-used starting material for the production of CNF is wood pulps.

Wood pulps are produced world-wide in large volumes and is a renewable commodity used in paper, packaging, hygiene products, textiles. The global production of wood pulps was estimated at 144 million tonnes in 2019 (FAO 2016). Wood pulps are composed separated anatomical plant fibres enriched in cellulose, by depletion of its lignin and hemicellulose contents during the pulping process. The fibre-wall of a pulp fibre contain cellulose in a complex hierarchical arrangement (Fengel and Wegener 1989), with cavities (or pores) resulting from the removal of lignin and hemicelluloses. Wood and wood pulps has been the subject of SAXS studies, examples are; Jakob et al. 1995, Lichtenegger et al. 1999, Fink. et al 2004, Jungnikl et al. 2008, Virtanen et al. 2015, Mao et al. 2019.

The focus of this work is on cellulose obtained after pulping and is referred to as *isolated cellulose* emphasising it may be distinct from cellulose prior to pulping.

Cellulose isolated from wood exists as bundles of β-(1→4)-D-glucan polymers, in this work called *fibrils*. These Fibrils can aggregate into larger structures, in this work called *fibril aggregates*. Lateral and longitudinal dimensions of fibrils and fibril aggregates depend on the choice of the source material, the details of the pulping procedure, and the drying history of a cellulose-rich pulp. Fibril aggregates combine into larger morphological features of the fibre wall, eventually forming a fibre (Fengel and Wegener 1989).

In cellulose-rich fibres isolated from wood, the lateral dimensions of fibrils are typically a few nanometres (3 nm to 5 nm), and the lateral dimensions of fibril aggregates can be several tenths of nanometres depending on the isolation procedure and drying history of the material, Fig. 1.

Pores resulting from the removal of components during pulping can range in size from fractions of nanometres to several tenths of nanometres. Size-wise, the widths of cellulose fibrils, cellulose fibril aggregates and pores are in the size-range addressable by SAXS measurements. SAXS measurements can be performed on both dry and water swollen fibre samples, where the dry and swollen states of the same material show large structural differences, Fig. 2.

One characteristic of cellulose-rich pulps is their fibre saturation point (FSP) which describes the maximum amount of water that can be accommodated by the pore system in the fibre wall, relative to the solids content (Stone and Scallan 1967). For cellulose-rich pulps isolated from wood, the FSP is typically around the value of 1 (mass water divided by mass solids). Effectively, the FSP value describes the maximum ‘dilution’ of the fibre wall solids that can be achieved while maintaining a fibre. The fibre wall of a cellulose-rich fibre is held together by strong and abundant interactions between cellulose fibrils, interactions strong enough to withstand the swelling pressure when in a water swollen state.

In cellulose rich fibres, cellulose fibrils are high aspect ratio particles arranged into a complex hierarchical fibre wall structure, with high a degree of local fibril alignment in a major part of the fibre wall (Fengel and Wegener 1989), an alignment that result in strong and abundant interactions between neighbouring fibrils promoting the formation of cellulose fibril aggregates, with an associated distribution in fibril aggregate widths. In brief, the interior of a cellulose rich fibre wall can be described as a dense network where cavity-sizes, widths, and lengths of the solid segments of the network all are associated with high degrees of variability. Interpreting SAXS data recorded on cellulose-rich pulps presents a challenge. Furthermore, strong, and abundant interactions combined with large degrees of variability in the structural features makes it difficult to separate recorded SAXS signals into contributions from form factors and structure factors (Porod 1982) even in the water swollen, most ‘diluted’, case.

Even in the case where ‘dilution’ could reach values higher than the FSP becomes futile since this would imply partial or complete removal of the structural features targeted for investigation.

In this work, an alternate strategy was attempted for the interpretation of SAXS data recorded on cellulose-rich fibres. Starting from a conceptual model representing the main features of a cellulose-rich fibre wall with abundant interactions between fibrils, SAXS intensity profiles were simulated for different particle and pore sizes. Subsequently, experimental data were modelled as a superposition of simulated

SAXS intensity profiles. This way, it becomes possible to interpret the experimental SAXS data in terms of a small set of apparent average particle and apparent average pore sizes. The approach used in this work is in some respects like the work presented by Debye (Debye 1957). Results from modelling of experimental data is presented and CP/MAS ^{13}C-NMR data are supplied for comparison.

Experimental

Samples: All sample materials were initially dry. Dry samples were used after being exposed to ambient conditions for several days. Water swollen samples were placed in excess of deionized water overnight before sample preparation and measurement.

Table 1
Sample ID and descriptions, relative glucose contents, and fibre saturation point (FSP) of the samples used in this work. Values within parenthesis are standard deviations. The volumetric fill factor (volume of solids divided by total volume) was calculated from the FSP value assuming a cellulose density of 1500 kg/m^3.

Sample ID	Description	Relative glucose content (%)	Fibre saturation point (FSP, g/g)	Volumetric fill factor (F_F, m^3/m^3)
SWP	Pre-hydrolysed bleached softwood soda pulp	97	0.40 (0.08)	0.63 (0.05)
HWP	Eucalyptus sulphite dissolving pulp, 96α	97	0.68 (0.10)	0.50 (0.04)
Lint	Cotton linters	99	0.21 (0.08)	0.76 (0.07)

Carbohydrate composition: Carbohydrate composition was determined according to SCAN-CM 71:09 using a high-performance anion-exchange chromatography system, Dionex ISC-5000, coupled to a CarboPac PA1 (250 mm x 4 mm i.d.) column (Dionex, Sweden) and a pulsed amperometric detector (HPAEC-PAD). The uncertainty for the relative glucose content is +/- 20 %.

Fibre saturation point (FSP): Measurements were conducted in a manner similar to that of Stone and Scallan (Stone and Scallan 1967) but using only one high molecular mass dextran. Water swollen samples with a known solids content were mixed with a dextran solution of known concentration (approximately 1%, dextran mass/solution mass) in deionized water, approximately one (1) mass unit of wet sample mass being mixed with three (3) mass units of dextran solution. After mixing, the sample was stored in a sealed vessel at room temperature for three (3) days to equilibrate. A liquid sample was subsequently taken and filtered through a Puradisc syringe filter (Whatman, Maidstone, UK) equipped with a 0.45 µm polytetrafluoroethylene membrane in a polypropylene housing (VWR International AB, Stockholm, Sweden). The concentration of dextran in the sample was determined using a calibration curve established for the optical rotation of polarized light measured using a Polartronic M100 Touch polarimeter (Schmidt + Haensch GmbH & Co., Berlin, Germany) operating at 589 nm, with a resolution of

0.001° (angular degree) and a precision of ± 0.005° at 589 nm. The calibration curve was computed using three dextran concentrations: approximately 0.5, 1.0 and 1.5% (dextran mass/solution mass), covering the range of all measurements. Dynamic light scattering was used to determine the hydrodynamic diameter of the dextran molecules (Dextran 1500–2800, CAS No. 9004-54-0) at high dilution in deionized water (Zetasizer ZEN3600; Malvern Instruments Ltd., Malvern, UK), using a He-Ne 4.0 mW, 633 nm laser and a detector angle of 178°. The hydrodynamic diameter of the dextran molecules was found to be 97 ± 2 nm with a polydispersity index of 0.2, measured at a dextran concentration of 0.15 g per L solution. Based on the determined size of the dextran, the results obtained for the FSP were interpreted as representing liquid contained in pores smaller than approximately 97 nm in diameter. The FSP value is expressed as the dimensionless ratio of the mass of pore water to the mass of dry solids (g/g).

SAXS: X-ray measurements were performed on an Anton Paar SAXSpoint 2.0 system (Anton Paar, Graz, Austria) equipped with a Microsource x-ray source (Cu Kα radiation, wavelength 0.15418 nm) and a Dectris 2D CMOS Eiger R 1M detector with 75 µm by 75 µm pixel size. All measurements were performed with a beam size of about 500 µm in diameter, at a sample stage temperature of 25°C with a beam path pressure at 1–2 mBar. For SAXS measurements, the sample to detector distance (SDD) was SDD = 562 mm. Water swollen samples were mounted on a Multi-paste Holder mounted on a Heated Sampler and a VarioStage (Anton Paar, Graz, Austria). Water swollen samples were kept between Kapton foils in hermetically sealed compartments and were not exposed to vacuum during measurement. Dry samples were mounted on a Solids Sampler Holder mounted on a VarioStage (Anton Paar, Graz, Austria). The dry samples were exposed to the vacuum in the beam path. For dry sample, 6 frames each of 5 minutes duration were recorded, giving a total measurement time of 30 minutes per sample. For wet samples 10 frames of 6 minutes duration were recorded, giving a total measurement time of 1 hour per sample. For all samples, the transmittance was determined and used for scaling of the scattering intensities. For wet samples, scattering data recorded on deionized water with the same experimental setup was used for background subtraction. Binning was used to generate graphs with between 500 to 510 data points, which were used for graphs and modelling. The software used for instrument control was SAXSdrive version 2.01.224 (Anton Paar, Graz, Austria), and post-acquisition data processing was performed using the software SAXSanalysis version 3.00.042 (Anton Paar, Graz, Austria).

CP/MAS ^{13}C-NMR: Cross-Polarization Magic Angle Spinning Carbon-13 Nuclear Magnetic Resonance Spectra. All samples were packed uniformly in a zirconium oxide rotor. Water swollen samples had a water content of 40 % to 60 %. The CP/MAS ^{13}C-NMR spectra were recorded in a Bruker Avance III AQS 400 SB instrument operating at 9.4 T. All measurements were carried out at 295 (± 1) K with a magic angle spinning (MAS) rate of 10 kHz. A 4-mm double air-bearing probe was used. Data acquisition was performed using a cross-polarization (CP) pulse sequence, i.e., a 3.15 microseconds proton 90-degree pulse, 800 microseconds ramped (100–50 %) falling contact pulse, with a 2.5 s delay between repetitions. A SPINAL64 pulse sequence was used for ^{1}H decoupling. The Hartmann-Hahn matching procedure was based on glycine. The chemical shift scale was calibrated to the TMS-scale (tetramethylsilane, $(CH_3)_4Si$) by assigning the data point of maximum intensity in the alpha-glycine

carbonyl signal to a shift of 176.03 ppm. 4096 transients were recorded on each sample leading to an acquisition time of about 3 h. The software for spectral fitting was developed at Innventia AB and is based on a Levenberg-Marquardt algorithm (Larsson 1997). All computations were based on integrated signal intensities obtained from spectral fitting (Wickholm 1998). The errors given for parameters obtained from the fitting procedure are the standard error with respect to the quality of the fit.

Computations: All Simulations were performed using software written in C++ utilizing parallelization. Simulations were executed on desktop PC computers, operating system Microsoft Windows® 10, running multi-core CPUs (AMD Ryzen® 7 3700X or AMD Ryzen® 9 3900X). Typical simulation times were between one to one and a half hours, depending on input parameters. Computational details are given in Supplementary Information (SI).

Results And Discussions

For comparison purposes, CP/MAS ^{13}C-NMR spectra were recorded on the water swollen samples, Fig. 3. Estimates of the average lateral fibril dimension (LFD) and the average lateral fibril aggregate dimension (LFAD) from CP/MAS ^{13}C-NMR spectra, based on the method by Larsson and Wickholm (Larsson et al. 1997, Wickholm et al 1998) are given in Table 2.

Table 2
The average lateral fibril dimensions (LFD) and the average lateral fibril aggregate dimensions (LFAD) determined from CP/MAS ^{13}C-NMR spectra recorded on dry and water swollen samples. Values within parenthesis are standard errors. LFAD cannot be measured in dry samples by the used CP/MAS ^{13}C-NMR method.

Sample ID	LFD (nm)	LFAD (nm)
SWP	4.7 (0.1)	32 (1)
HWP	4.4 (0.1)	27 (1)
Lint	7.0 (0.2)	37 (2)

Small angle X-ray data was recorded on water swollen and dry samples and the recorded SAXS data was modelled using a simulation model described in detail in the Supplementary Information (SI). Here only a brief account of the main features of the simulation model are given.

The simulation of SAXS intensity profiles was based on a conceptual representation of the distribution of cellulose fibrils and fibril aggregates in the fibre wall, which is illustrated in Fig. 4. The model is conceptual in the sense that it was only used as a route to design the algorithm used for generating electron density paths.

Once a sufficient number of electron density paths was simulated, discrete versions of the spatial correlation function (SCF) and the pair distance distribution function (PDDF) was calculated and subsequently simulated SAXS intensity profiles, $I_k(q)$ in Equation [1], was generated. The modelling of experimental SAXS data, $I_{EXP}(q)$, was performed by superposition of simulated SAXS intensity profiles $I_k(q)$ weighted by W_k, with the addition of a modelling parameter describing any instrument background intensity b:

$$I_{EXP}(q) \approx \sum_k w_k I_k(q) + b$$

The advantage of the simulation method was that it made it possible to associate each simulated intensity profile with an apparent average particle size (AAPS) and an apparent average cavity size (AACS), connecting each intensity profile to a length scale characteristic of the structures in the sample material. Here, the concept of cavity was used to describe interstitial spaces between solid particles whether filled with water or evacuated. For all samples used in this study, three intensity components (six adjustable model parameters plus one background intensity) were used to model the experimental SAXS data.

Figure 5 shows the results from modelling SAXS data recorded on dry samples; Figure 6 shows the results from modelling SAXS data recorded on the corresponding water swollen samples. Modelling parameters are shown in Table 3 (dry samples) and Table 4 (water swollen samples).

Table 3. Summary of the modelling parameters used for the dry samples. Experimental data was modelled by use of three intensity components, I_1, I_2, I_3 (Equation [1]) for all dry samples. Modelling was performed by adjusting the component weights, w_k, and the real space step size, Dx_k, for each intensity component. The “larger than” arrow in the table indicates modelling of structures too large to be unambiguously assigned using the q-range of the experimental data. The sum of squared relative residuals (SSRR) is given as an indicator of the quality of the fit. See Supplementary Information for details.

SWP						
	w_k (%)	Dx_k (pm)	AAPS (nm)	AACS (nm)	*b*	SSRR
I_1	76 (3)	150 (10)	> 322 (110)	> 36 (12)	0.26 (0.01)	1.98
I_2	5 (1)	13 (2)	28 (10)	3.1 (1.1)		
I_3	19 (1)	4.6 (0.2)	9.9 (3.4)	1.1 (0.4)		
HWP						
I_1	78 (4)	150 (10)	> 330 (113)	> 37 (13)	0.62 (0.03)	1.00
I_2	3 (1)	17 (5)	36 (12)	4.0 (1.4)		
I_3	20 (1)	4.3 (0.1)	9.1 (3.1)	1.0 (0.3)		
Lint						
I_1	64 (2)	210 (5)	> 460 (157)	> 51 (17)	0.3 (0.02)	1.66
I_2	23 (1)	11.0 (0.2)	24 (8)	2.6 (0.9)		
I_3	14 (1)	3.7 (0.3)	7.9 (2.7)	0.9 (0.3)		

Table 4. Summary of the modelling parameters used for the water swollen samples. Experimental data was modelled by use of three intensity components, I_1, I_2, I_3 (Equation [1]) for all water swollen samples. Modelling was performed by adjusting the component weight, w_k, and the real space step size, Dx_k, for each intensity component. The “larger than” arrow in the table indicates modelling of structures too large to be unambiguously assigned using the q-range of the experimental data. The sum of squared relative residuals (SSRR) is given as an indicator of the quality of the fit. See Supplementary Information for details.

SWP						
	w_k (%)	Dx_k (pm)	AAPS (nm)	AACS (nm)	b	SSRR
I_1	3.9 (0.3)	100 (4)	> 72 (20)	> 42 (12)	0.16 (0.01)	4.71
I_2	5.8 (0.3)	20 (4)	14 (4)	8.4 (2.3)		
I_3	90 (6)	6.6 (0.1)	4.7 (1.3)	2.8 (0.8)		
HWP						
I_1	4.9 (0.3)	100 (10)	> 48 (13)	> 48 (13)	0.31 (0.05)	7.74
I_2	10 (1)	14.5 (0.3)	6.9 (1.8)	6.9 (1.8)		
I_3	85 (6)	5.6 (0.1)	2.7 (0.7)	2.7 (0.7)		
Lint						
I_1	5.0 (0.2)	70 (2)	> 82 (24)	> 26 (8)	0.27 (0.02)	7.77
I_2	23 (1)	14 (1)	16 (5)	5.2 (1.5)		
I_3	73 (3)	7.8 (0.2)	9.1 (2.7)	2.9 (0.9)		

The values of the weights for the three simulated superposition components (I_1, I_2, and I_3 in Table 3 and Table 4) used to model the recorded SAXS data are charted in Fig. 7. Although the length-scales (Δx_k in Table 3 and Table 4) are not identical between samples, the three superposition components are coarsely viewed as representing the abundance of larger (I_1), intermediate (I_2) and smaller (I_3) structural features in the samples.

The FSP values and consequently the volumetric fill factors were determined for the water swollen samples. For the dry samples, the volumetric fill factor cannot be determined by FSP measurements since it implies swelling of the sample. For this reason, the volumetric fill factor was set to a value of 0.9, corresponding to an FSP value of about 0.07. Cellulose-rich fibres conditioned in ambient conditions (23 °C, 50 % RH) typically contains between 5 % to 10 % water. The same volumetric fill factor was applied to length scales, since only one FSP value was available for each sample.

Literature values for the density of cellulose rich fibres are available, for cotton fibres density values of 1540–1570 kg/m^3 has been reported (Temming 1973). However, this is a density value close to that of cellulose I, implying a complete lack of cavities in a dry cotton fibre wall. This is contradictory to SAXS data (e.g. the experimental data recorded on the dry Lint sample in Fig. 5) where a signal is visible in the q-range 0.6 nm^{-1} to 0.8 nm^{-1}, indicating a significant presence of non-uniformity in the electron density, consistent with the presence of cavities.

Using SAXS and CP/MAS ^{13}C-NMR for nano-structural characterization of cellulose rich pulps, the differences in the principles of operation of SAXS and CP/MAS ^{13}C-NMR opens the possible to obtain complementary information when applying the two techniques the same sample. The interpretation for the samples in this study was that the modelled I_3 components related to size-ranges associated with lateral fibrils dimensions, corresponding to the LFD measures obtained from CP/MAS ^{13}C-NMR. Similarly, the interpretation of the I_2 components was that they were related to the lateral dimensions associated with fibril aggregates, corresponding to the LFAD measures obtained from CP/MAS ^{13}C-NMR. The modelled I_1 components, corresponded to structural features too large to be unambiguously assigned by either the SAXS technique or the CP/MAS ^{13}C-NMR technique, the way they were used in this work.

In Fig. 7, the three dry samples SWP, HWP and Lint all showed dominating large structures, as modelled by the I_1 components, that gave a considerable signal intensity contribution in the observable q-range. These structural features were too large to be unambiguously assigned by the used experimental setup, this is indicated in Table 3 and Table 4 by a “larger than” symbol. In all the investigated dry samples the largest relative component weight (w_k) was observed for the I_1 components. This agreed with expectations, cellulose fibrils aggregate into larger structures as a consequence of drying, which contributes to hornification (Krässig 1993).

Less abundant smaller structures were observed when modelling the dry sample’s experimental SAXS intensities. The AAPS corresponding to the intensity component I_2 were found to be in a size range similar to the size range of the LFAD measured by CP/MAS ^{13}C-NMR recorded on water swollen samples, Table 2, though no direct correlation between samples was found.

The AAPS related to the intensity component I_3 showed the presence of particles larger than the LFD measured by CP/MAS ^{13}C-NMR on water swollen samples. One possible reason for this is illustrated in Fig. 8. If, during drying, intimate local aggregation of fibrils occur, this could lead to local removal of cavities (electron density contrast) between fibrils, yielding SAXS AAPS representing partial fibril aggregates. One interesting finding was that all modelling results of the SAXS data of dry samples contained an I_3 component associated with AAPS’s significantly smaller than the LFAD (CP/MAS ^{13}C-NMR, water swollen samples) and AACS’s in the range of 1 nanometre. This indicates the existence of porosity of the cellulose structure also in the dry state, consistent with the materials known ability to rapidly re-swell.

In cases where intimate proximity between fibrils reduces the electron density contrast to the point where a SAXS measurement may not distinguish the width of individual fibrils, distinct fibril surfaces polymer conformations may still be present, allowing for CP/MAS ^{13}C-NMR to distinguish fibrils also in the dry samples. As shown in Fig. 9 the signal positions interpreted to originate from carbon-13 nuclei at the C4 and the C6 positions of the anhydroglucose units in fibril surface polymers occur at the same average positions in spectra recorded on dry and water swollen samples, though significantly broadened in the cases of dry samples.

Common to all water swollen samples, SWP, HWP and Lint, in Fig. 7 was an increased abundance of smaller structural features as a consequence of swelling, compared with their dry counterparts. This agrees with expectations, swelling increase the specific surface area and increases the abundance and size of cavities in cellulose rich fibres, accompanied by an increased electron density contrast at smaller length scales.

In the cases of water swollen samples, the SAXS modelling results showed a significantly smaller abundance of the intensities originating from structures too large to be unambiguously assigned (relative weight of component I_1) compared with their dried counterparts (Fig. 7 and Table 3 and Table 4). For intensity components, I_2 and I_3 in Table 4, the ranking of the samples' AAPS was in the order Lint > SWP > HWP, in agreement with the sample ranking based on the CP/MAS ^{13}C-NMR LFD and LFAD measured on water swollen samples, Table 2.

For the water swollen samples, comparing the AAPS for the I_2 intensity components (Table 4) with the CP/MAS ^{13}C-NMR LFAD measures (Table 2), the modelling of SAXS results showed AAPS consistently smaller that the corresponding LFAD. One interpretation of this observation could be that the SAXS measurements could detect cavities within cellulose fibril aggregate, cavities that the CP/MAS ^{13}C-NMR measurements could not distinguish. Some support for this interpretation can be found in previous results obtained by NMR relaxometry data (Larsson 2017), where probing the cellulose specific surface area (particle surface-to-volume ratio) by ^{2}H-relaxation measurements showed results intermediate between the extremes obtainable from CP/MAS ^{13}C-NMR results. Consistent with the hornification behaviour cellulose, discussed above, if part of the structures illustrated in the right panel of Fig. 8, remain after re-swelling in water this can result in a structure inside fibril aggregates that is not compact, Fig. 10.

The SWP and HWP samples were produced by two different isolation procedure, the SWP was produced by an alkaline pulping process, while the HWP was produced by a comparatively more acidic pulping process. This may be an explanation for the differences observed in the modelling results for the two samples.

Conclusions

A method was developed for modelling SAXS data recorded on dense two-component systems with abundant interactions, cellulose rich pulps. The modelling method was independent of the establishments of form factors and structure factors and was applicable to dense samples with abundant interactions. Experimental SAXS data could be modelled using a limited number of simulated intensity components, and gave results, apparent average particle sizes (AAPS) in qualitative agreement with CP/MAS ^{13}C-NMR data recorded on the same samples. In the case of water swollen samples, SAXS modelling results and NMR data agreed on the ranking of particle sizes. The time necessary for simulations could be reduced by rescaling of simulated autocorrelation functions, due to their

independence of the choice of real space step size. This way a single autocorrelation function simulated for a specific sample could be used to generate SAXS intensity profiles corresponding to all length scales for that sample and used for efficient modelling of experimental data recorded on that sample.

Declarations

Acknowledgements

‘Stiftelsen Nils och Dorthi Troëdssons forskningsfond’ are gratefully acknowledged for funding; application 943/18, Development of interpretation models for Small Angle X-ray Scattering measurements of cellulose materials.

Funding (information that explains whether and by whom the research was supported)

‘Stiftelsen Nils och Dorthi Troëdssons forskningsfond’ are gratefully acknowledged for funding; application 943/18, Development of interpretation models for Small Angle X-ray Scattering measurements of cellulose materials

Conflicts of interest/Competing interests (include appropriate disclosures)

None

Availability of data and material (data transparency)

Can be supplied by corresponding author on request.

Code availability (software application or custom code)

Can be supplied corresponding author on request.

Authors' contributions (optional: please review the submission guidelines from the journal whether statements are mandatory)

Per Tomas Larsson: Idea, application for funding, planning of work, sample selection and supply, programming, and program development, performing numerical simulations, writing manuscript.

Jasna Stevanic-Srndovic: experimental work, FSP, scattering and CP/MAS ^{13}C-NMR measurements and post-acquisition processing of data.

Stephan Roth: Scientific discussions during theoretical development and discussions of simulation results, input on manuscript.

Daniel Söderberg: Scientific discussions during theoretical development and discussions of simulation results, input on manuscript.

Additional declarations for articles in life science journals that report the results of studies involving humans and/or animals

Not applicable

Ethics approval (include appropriate approvals or waivers)

No ethical conflicts exist.

Consent to participate (include appropriate statements)

All authors of this manuscript have participated in the work willingly.

Consent for publication (include appropriate statements)

All authors of this manuscript give their consent to publish the presented manuscript.

References

1. Brett CJ, Montani S, Schwartzkopf M, van Benthem RATM, Jansen JFGA, Griffini G, Roth SV, Johansson MK (2020). Revealing structural evolution occurring from photo-initiated polymer network formation. Communications Chemistry, 3(1), 1-7. doi.org/10.1038/s42004-020-0335-9.
2. Debye P, Anderson HR, and Brumberger H (1957). Scattering by an Inhomogeneous Solid II. The Correlation Function and Its Application. Journal of Applied Physics 28:679-683. doi.org/10.1063/1.1722830.
3. FAO, Food and Agriculture Organization of The United Nations (2016), pulp and paper capacities, survey 2015-2020, Rome, Italy. Spread sheets with data is available at URL:http://www.fao.org/forestry/statistics/80571/en/.
4. Fengel D, Wegener G (1989). Chapters 2 and chapter 4 in Wood. Chemistry, Ultrastructure, Reactions. Walter de Gruyter, Berlin. doi.org/10.1515/9783110839654.
5. Fink HP, Weigel P, Ganster J, Rihm R, Puls J, Sixta H, Parajo JC (2004). Evaluation of new organosolv dissolving pulps. Part II: structure and NMMO processability of the pulps. Cellulose, 11(1), 85-98. doi.org/10.1023/B:CELL.0000014779.93590.a0.
6. Fratzl P (2003). Small-angle scattering in materials science-a short review of applications in alloys, ceramics, and composite materials. Journal of Applied Crystallography, 36(3), 397-404. doi.org/10.1107/S0021889803000335.
7. Geng L, Peng X, Zhan C, Naderi A, Sharma PR, Mao Y, Hsiao BS (2017). Structure characterization of cellulose nanofiber hydrogel as functions of concentration and ionic strength. Cellulose, 24(12), 5417-5429. doi.org/10.1007/s10570-017-1496-2.
8. Håkansson KM, Fall AB, Lundell F, Yu S, Krywka C, Roth SV, Santoro G, Kvick M, Prahl Wittberg L, Wågberg L, Söderberg LD. (2014). Hydrodynamic alignment and assembly of nanofibrils resulting in

strong cellulose filaments. Nature communications, 5(1), 1-10. doi.org/10.1038/ncomms5018

9. Jakob HF, Fratzl P, Tschegg SE (1994). Size and arrangement of elementary cellulose fibrils in wood cells: a small-angle X-ray scattering study of Picea abies. Journal of Structural Biology, 113(1), 13-22. doi.org/10.1006/jsbi.1994.1028.
10. Jakob HF, Fengel D, Tschegg SE, Fratzl P (1995). The elementary cellulose fibril in Picea abies: comparison of transmission electron microscopy, small-angle X-ray scattering, and wide-angle X-ray scattering results. Macromolecules, 28(26), 8782-8787. doi.org/10.1021/ma00130a010.
11. Jakob HF, Tschegg SE, Fratzl P (1996). Hydration dependence of the wood-cell wall structure in Picea abies. A small-angle X-ray scattering study. Macromolecules, 29(26), 8435-8440. doi.org/10.1021/ma9605661.
12. Jungnikl K, Paris O, Fratzl P, Burgert I (2008). The implication of chemical extraction treatments on the cell wall nanostructure of softwood. Cellulose, 15(3), 407. doi.org/10.1007/s10570-007-9181-5.
13. Keckes J, Burgert I, Frühmann K, Müller M, Kölln K, Hamilton M, Burghammer M, Roth SV, Stanzl-Tschegg S, Fratzl P (2003) Cell-wall recovery after irreversible deformation of wood. Nature materials, 2(12), 810-813. doi.org/10.1038/nmat1019.
14. Krässig HA (1993). Chapter 2 in Cellulose. Structure, Accessibility and Reactivity, Polymer Monographs Volume 11, Gordon and Breach Science Publishers, Amsterdam. doi.org/10.1002/pi.1995.210360114.
15. Larsson, PT, Wickholm K, Iversen T (1997). A CP/MAS ^{13}C-NMR investigation of molecular ordering in celluloses. Carbohydrate Research 302:19-25. doi.org/10.1016/S0008-6215(97)00130-4.
16. Larsson PT, Karlsson RMP, Westlund PO, Wågberg L (2017). The internal structure of isolated cellulose I fibril aggregates in the water swollen state. ACS Symposium Series book: Nanocelluloses: Their Preparation, Properties, and Applications, Editor(s): Umesh P. Agarwal, Rajai H. Atalla, and Akira Isogai, Volume 1251, Chapter 5, pp 91-112. doi.org/10.1021/bk-2017-1251.ch005.
17. Lichtenegger H, Müller M, Paris O, Riekel C, Fratzl P (1999). Imaging of the helical arrangement of cellulose fibrils in wood by synchrotron X-ray microdiffraction. Journal of applied crystallography, 32(6), 1127-1133. doi.org/10.1107/S0021889899010961.
18. Mao J, Heck B, Abushammala H, Reiter G, Laborie MP (2019). A structural fibrillation parameter from small angle X-ray scattering to quantify pulp refining. Cellulose, 26(7), 4265-4277. doi.org/10.1007/s10570-019-02386-0.
19. Mao Y, Liu K, Zhan C, Geng L, Chu B, Hsiao BS (2017). Characterization of nanocellulose using small-angle neutron, X-ray, and dynamic light scattering techniques. The Journal of Physical Chemistry B, 121(6), 1340-1351. doi.org/10.1021/acs.jpcb.6b11425.
20. Penttilä PA, Rautkari L, Österberg, M, Schweins R (2019). Small-angle scattering model for efficient characterization of wood nanostructure and moisture behaviour. Journal of applied crystallography, 52(2), 369-377. doi.org/10.1107/S1600576719002012.
21. Porod G (1982) Chapter 2, General Theory. In: in Small angle x-ray scattering, Glatter O and Kratky O (ed.) Academic Press, London, pp 17-52. doi.org/10.1002/actp.1985.010360520.

22. Pääkkö M, Ankerfors M, Kosonen H, Nykänen A, Ahola S, Österberg M, Ruokolainen J, Laine J, Larsson PT, Ikkala O, Lindström T. (2007). Enzymatic hydrolysis combined with mechanical shearing and high-pressure homogenization for nanoscale cellulose fibrils and strong gels. Biomacromolecules, 8(6), 1934-1941. doi.org/10.1021/bm061215p
23. Rosén T, Brouzet C, Roth SV, Lundell F, Söderberg LD (2018). Three-dimensional orientation of nanofibrils in axially symmetric systems using small-angle X-ray scattering. The Journal of Physical Chemistry C, 122(12), 6889-6899. doi.org/10.1021/acs.jpcc.7b11105.
24. Saito T, Kimura S, Nishiyama Y, Isogai A. (2007). Cellulose nanofibers prepared by TEMPO-mediated oxidation of native cellulose. Biomacromolecules, 8(8), 2485-2491. doi.org/10.1021/bm0703970
25. Stone JE, Scallan AM (1967). The effect of component removal upon the porous structure of the cell wall of wood II. Swelling in water and the fibre saturation point. Tappi 50(10):496–501.
26. Su Y, Burger C, Ma H, Chu B, Hsiao BS (2015). Exploring the nature of cellulose microfibrils. Biomacromolecules, 16(4), 1201-1209. doi.org/10.1021/bm501897z
27. Temming H, Grunert H (1973). Chapter 4, Data on the Chemistry and Physics of Cellulose, Temming-Linters, Peter Temming AG, Glückstadt, p 132.
28. Virtanen T, Penttilä PA, Maloney TC, Grönqvist S, Kamppuri T, Vehviläinen M, Serimaa R, Maunu SL (2015). Impact of mechanical and enzymatic pretreatments on softwood pulp fiber wall structure studied with NMR spectroscopy and X-ray scattering. Cellulose, 22(3), 1565-1576. doi.org/10.1007/s10570-015-0619-x
29. Wickholm K, Larsson PT, Iversen T (1998). Assignment of non-crystalline forms in cellulose I by CP/MAS ^{13}C-NMR spectroscopy. Carbohydrate Research 312:123-129. doi.org/10.1016/S0008-6215(98)00236-5.

Figures

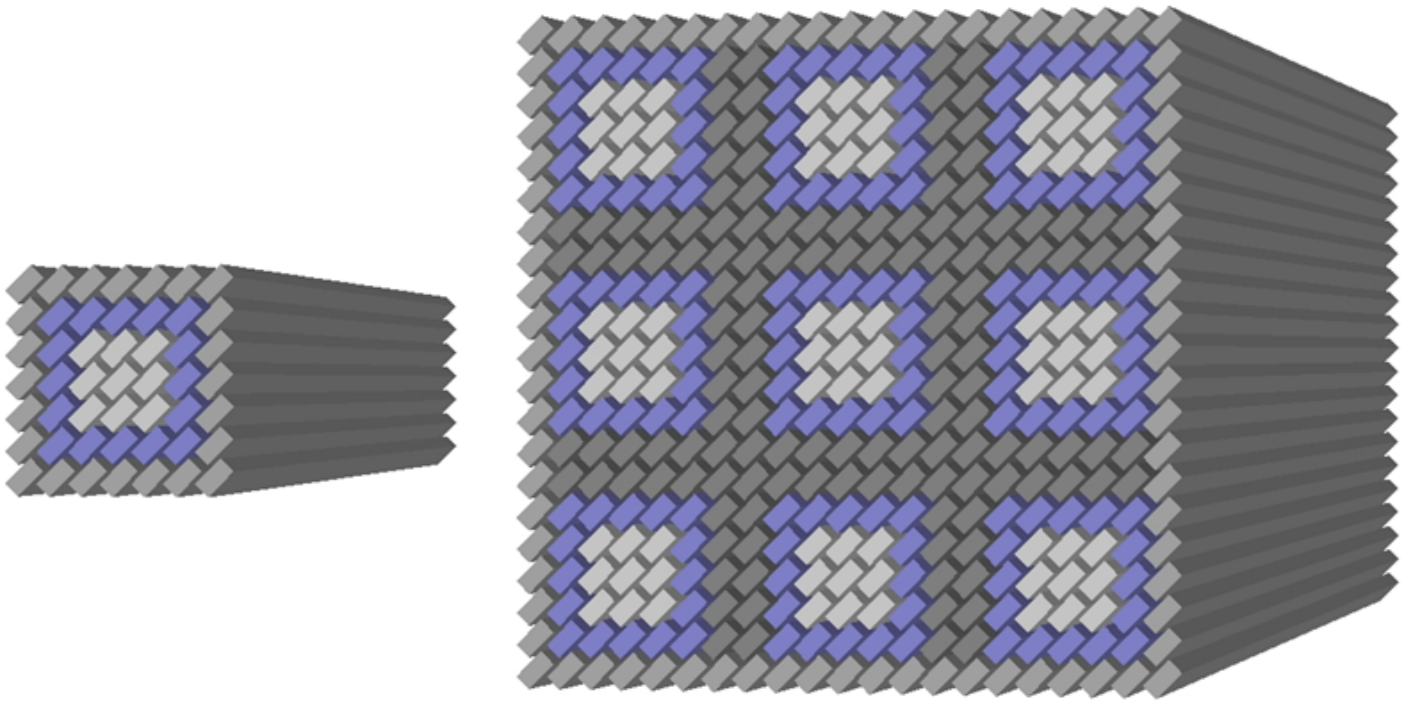

Figure 1

A simplified and idealized representation of a longitudinal segment of a cellulose fibril composed of 7-by-7 polymers (left), and a fibril aggregate comprising 3-by-3 fibrils (right). The ribbons represent polymers, grey: accessible surface polymers, blue: polymers in a para-crystalline form, light grey: polymers in the crystallin core, dark grey: inaccessible fibril surface polymers.

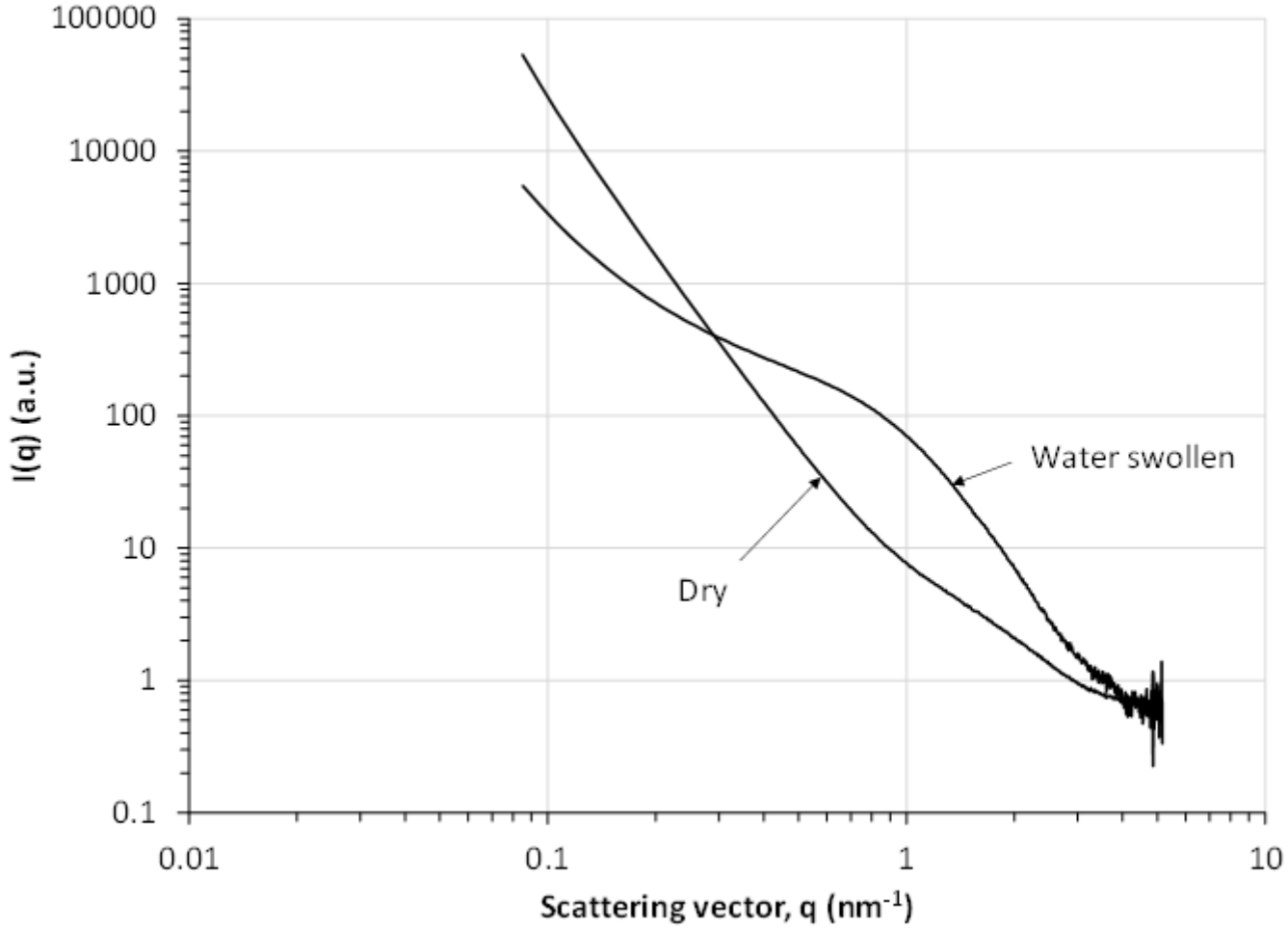

Figure 2

Scattering intensity I(q) as a function of the scattering vector q obtained from SAXS data recorded on a cellulose-rich pulp (sample HWP, see Experimental) in the water swollen and the dry state.

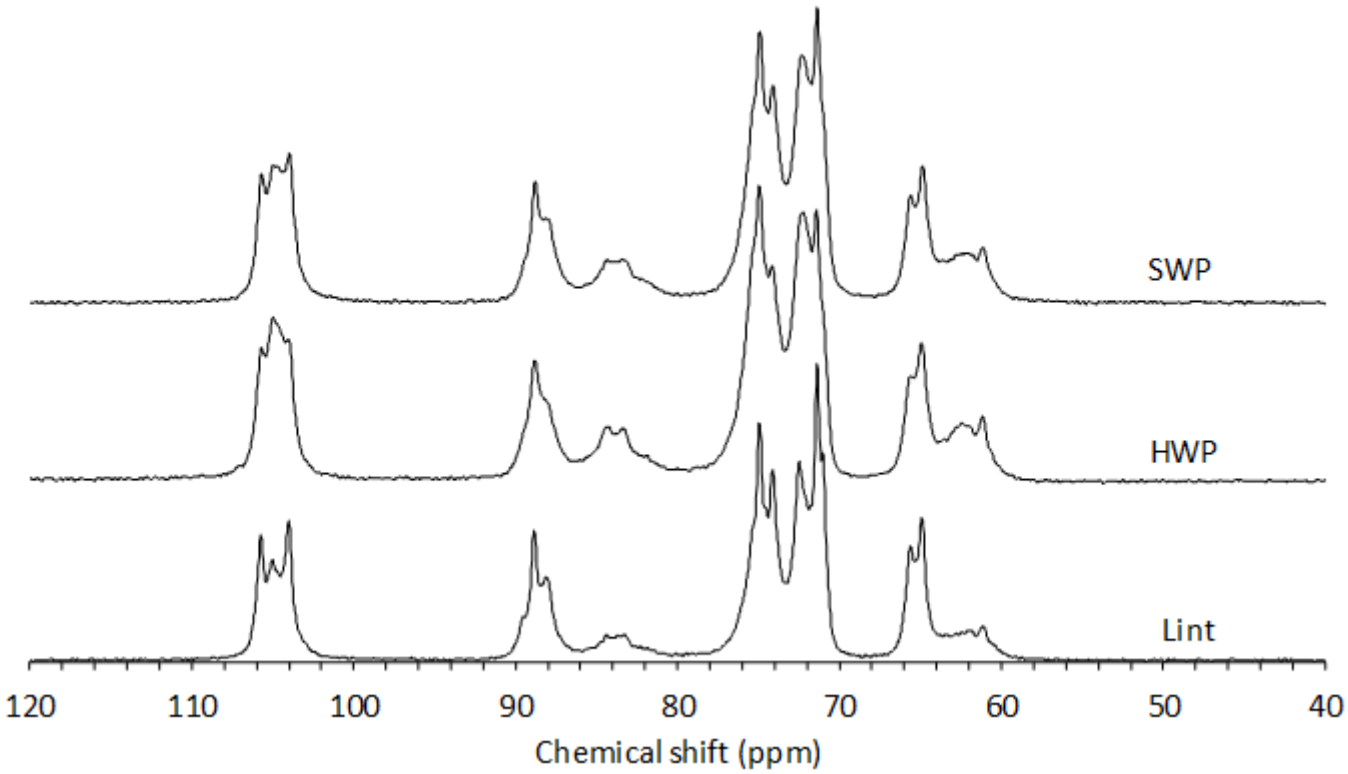

Figure 3

CP/MAS 13C-NMR spectra recorded on water swollen cellulose rich samples. Sample abbreviations in the figure are given in Table 1.

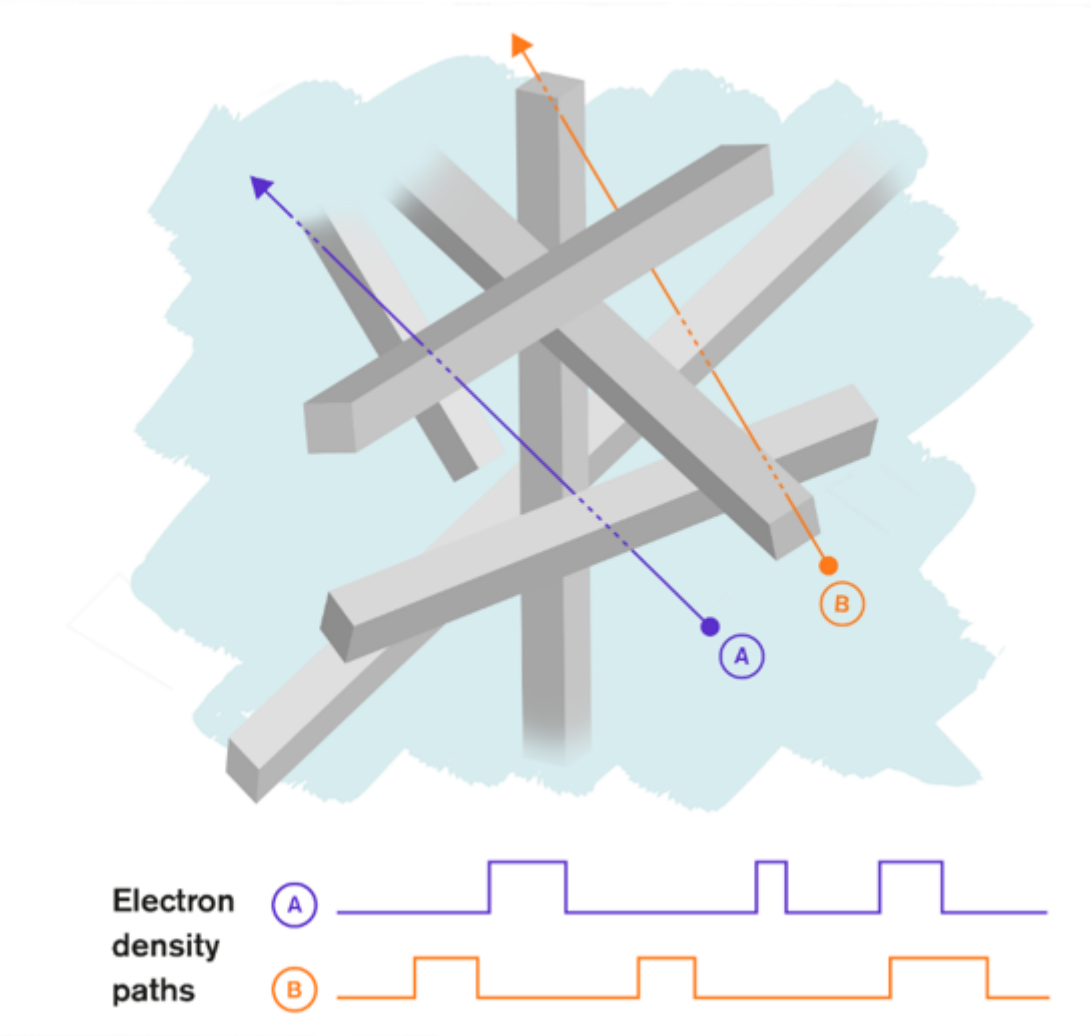

Figure 4

A conceptual image describing how an electron density path (EDP) can be visualized in a two-component sample, here the solid material is cellulose. The EDPs shown at the bottom illustrates two examples of electron density paths encountered when following path A or path B through the sample. The grey cuboids representing the solids was assigned a higher electron density value, and the interstitial spaces between the grey cuboids (vacuum or water) was assigned a lower electron density value. Depending on the size-range (q-range) of modelled data the grey cuboid can represent cellulose fibrils (widths about 3 nanometres to 5 nanometres) or cellulose fibril aggregates (widths in the range of ten to several tenths of nanometres).

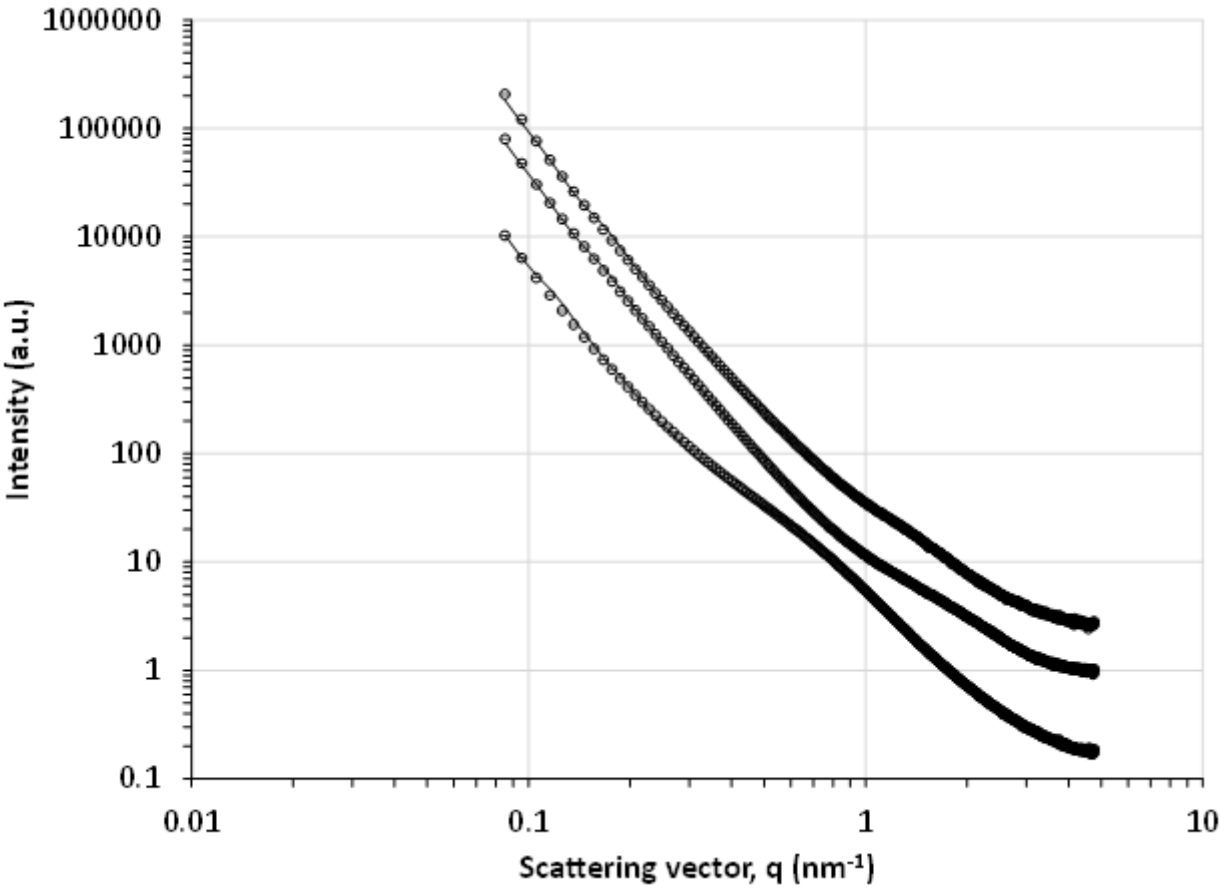

Figure 5

Modelling results for the dry samples. Solid lines represent the modelled intensity, circles represent experimental intensity. Error bars for the experimental intensity are plotted, in most cases error bars are covered by the markers. The scattering intensity has been arbitrarily scaled to minimize overlap of the curves. Top: SWP, middle: HWP, bottom Lint.

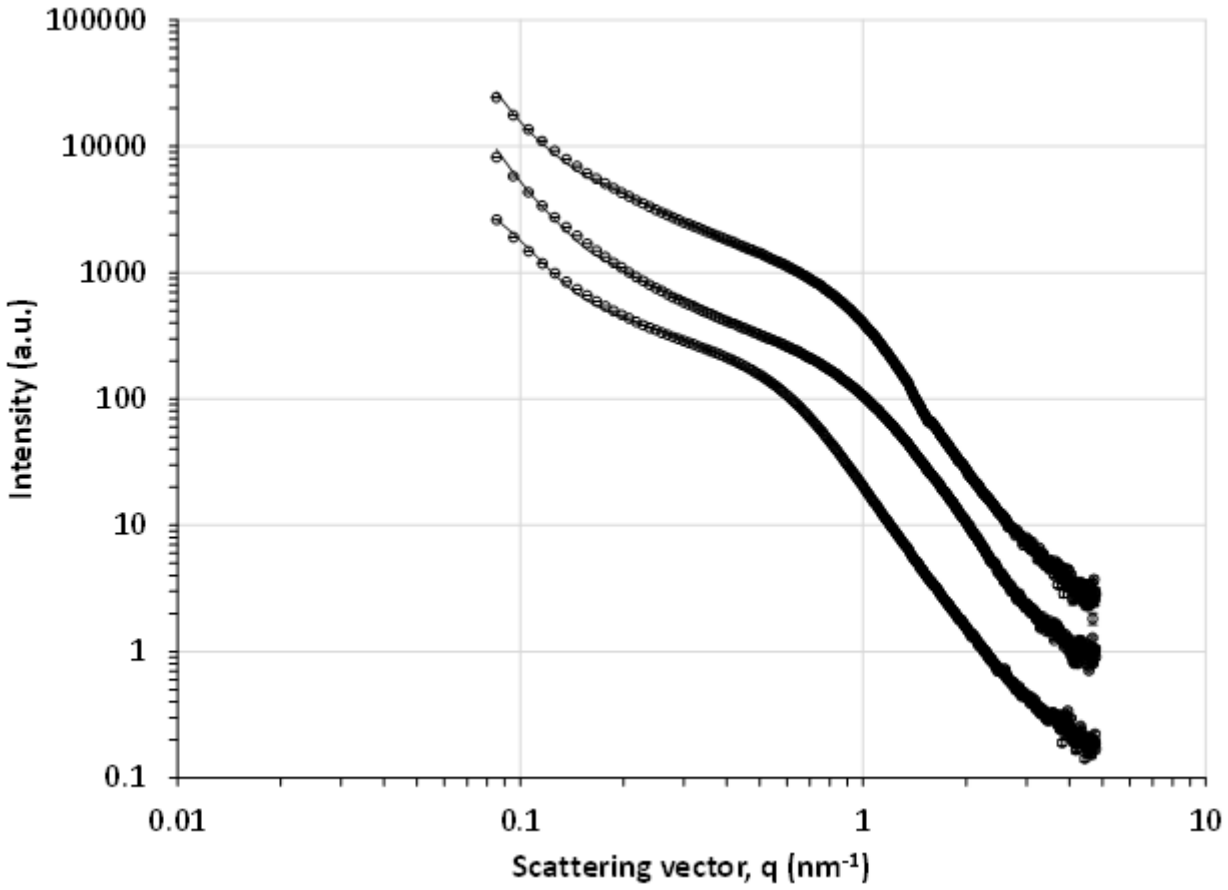

Figure 6

Modelling results for the water swollen samples. Solid line represents the modelled intensity, circles represent experimental intensity. Error bars for the experimental intensity are plotted, in most cases error bars are covered by the markers. The scattering intensity has been arbitrarily scaled to minimize overlap of the curves. Top: SWP, middle: HWP, bottom Lint. (The kink in the SWP experimental data at a q-value about 1.5 nm-1 is from the detector gap.)

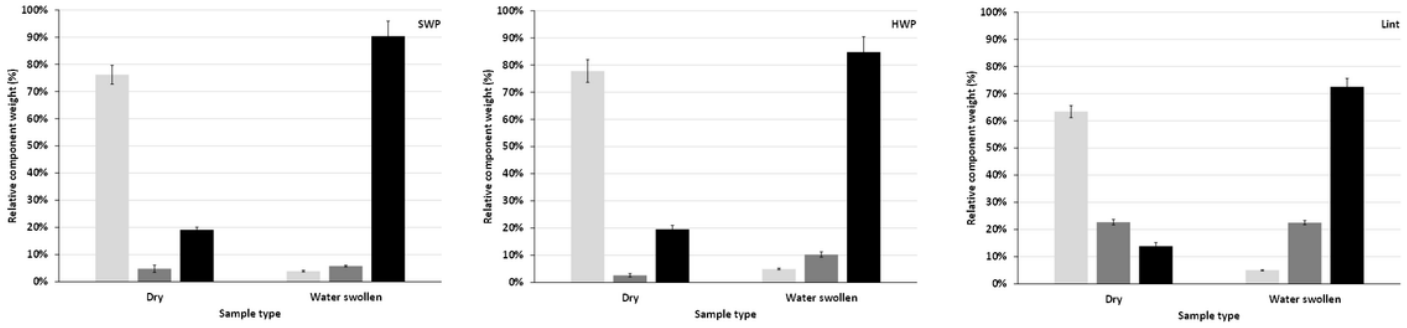

Figure 7

The values of the relative weights for the three simulated superposition components (I1, I2, and I3 in Table 3 and Table 4) used to model the recorded SAXS data. From top to bottom the samples are SWP, HWP and Lint. The inset in the upper right of each panel gives the sample name. The three superposition components were viewed as representing the abundance of larger (I1, light grey bars), intermediate (I2, grey bars), and smaller (I3, black bars) structural features in the samples.

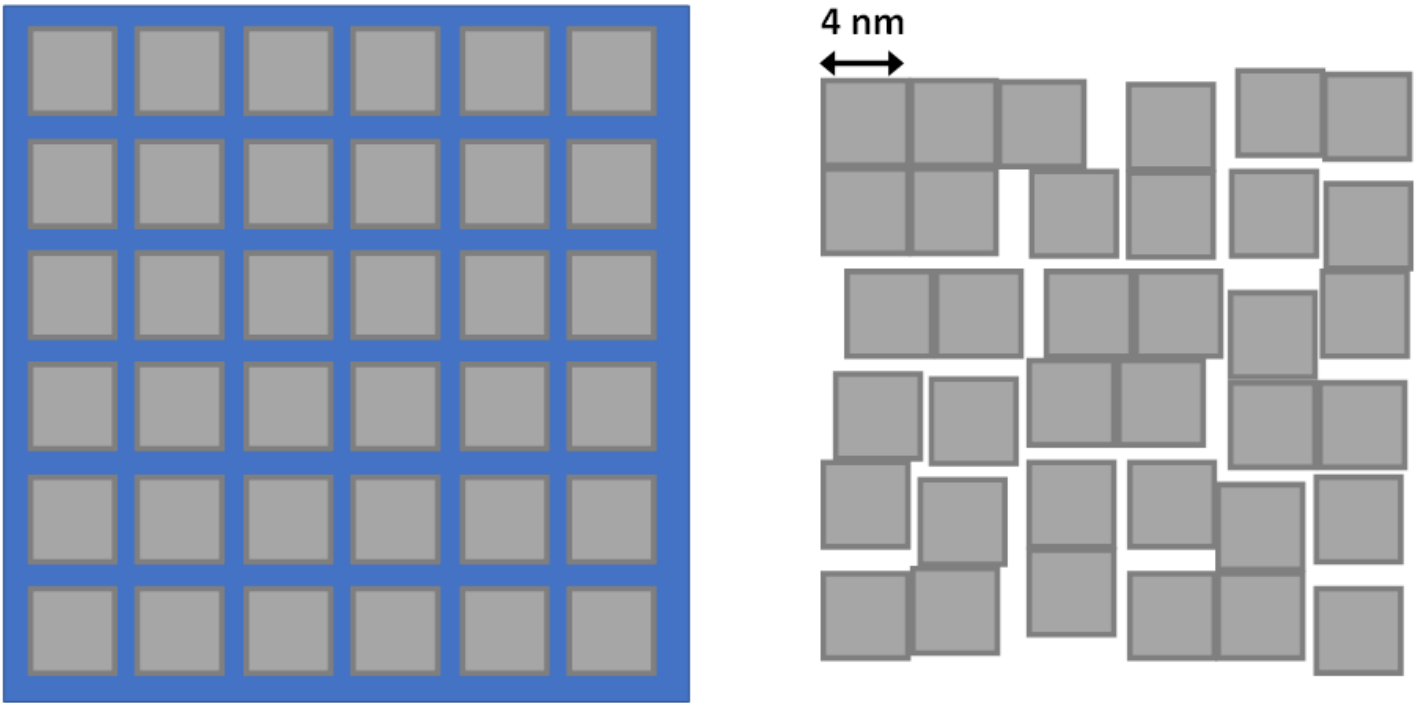

Figure 8

An idealized illustration of a cross-section of a fibril aggregate composed of 6-by-6 fibrils, each with a width of 4 nanometres. Left: idealized water swollen state, right: dry state. The aggregation pattern of cellulose fibrils may vary along the length direction of a fibril aggregate. The length direction is perpendicular to the plane of the illustrated cross-section (not shown).

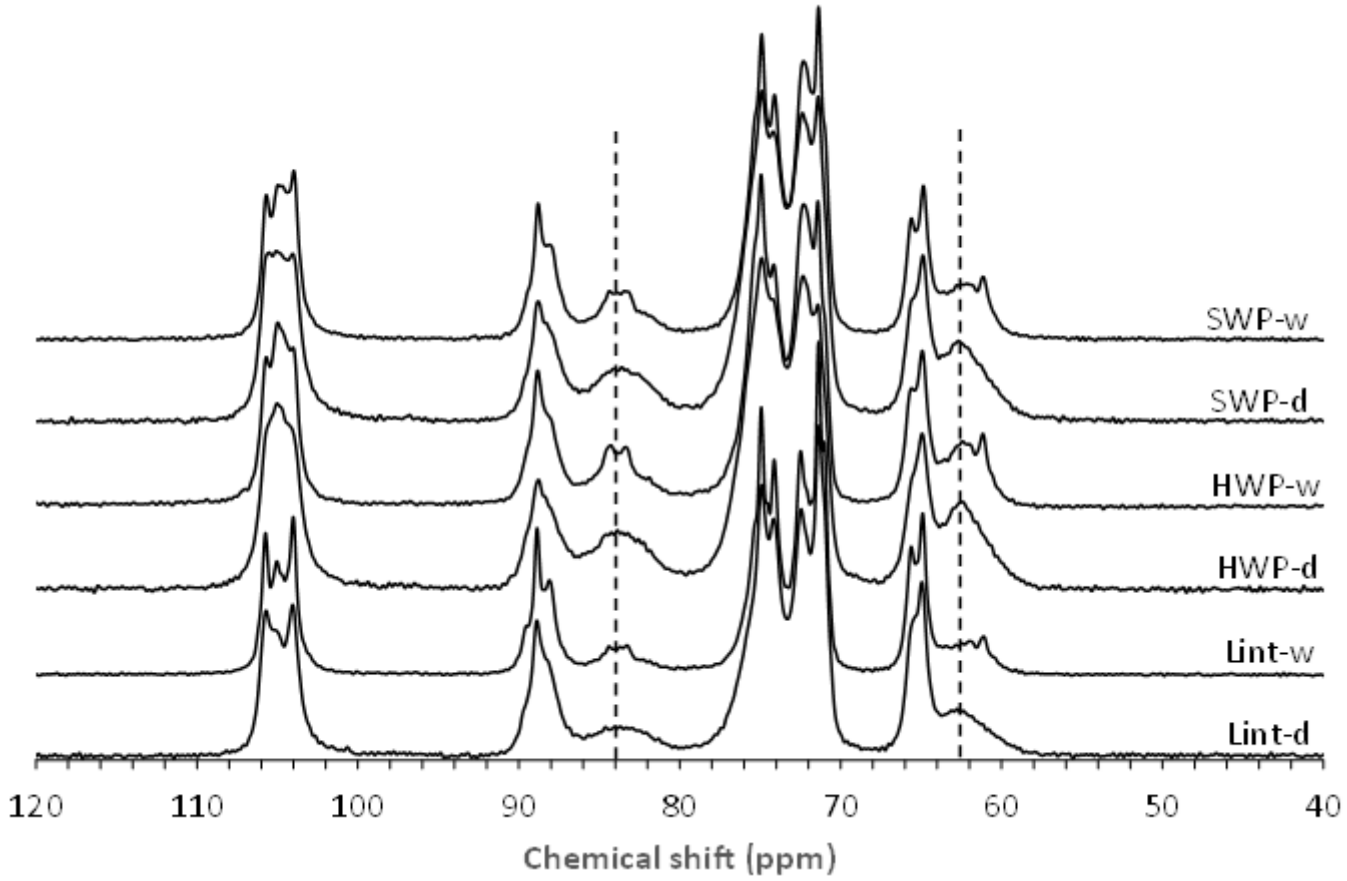

Figure 9

CP/MAS 13C-NMR spectra recorded on the samples in a dry (d) and water swollen (w) state. Signal intensity originating from fibril surface polymers is visible around 84 ppm to 83 ppm (anhydroglucose C4) and 63 to 60 ppm (anhydroglucose C6) in both dry and water swollen samples (positions indicated by broken vertical lines). The presence of separate signals originating from fibril surface polymers in both the dry and water swollen states indicates that the conformational differences between fibril core polymers and fibril surface polymers prevails independent of the degree of compactness of the fibril aggregates.

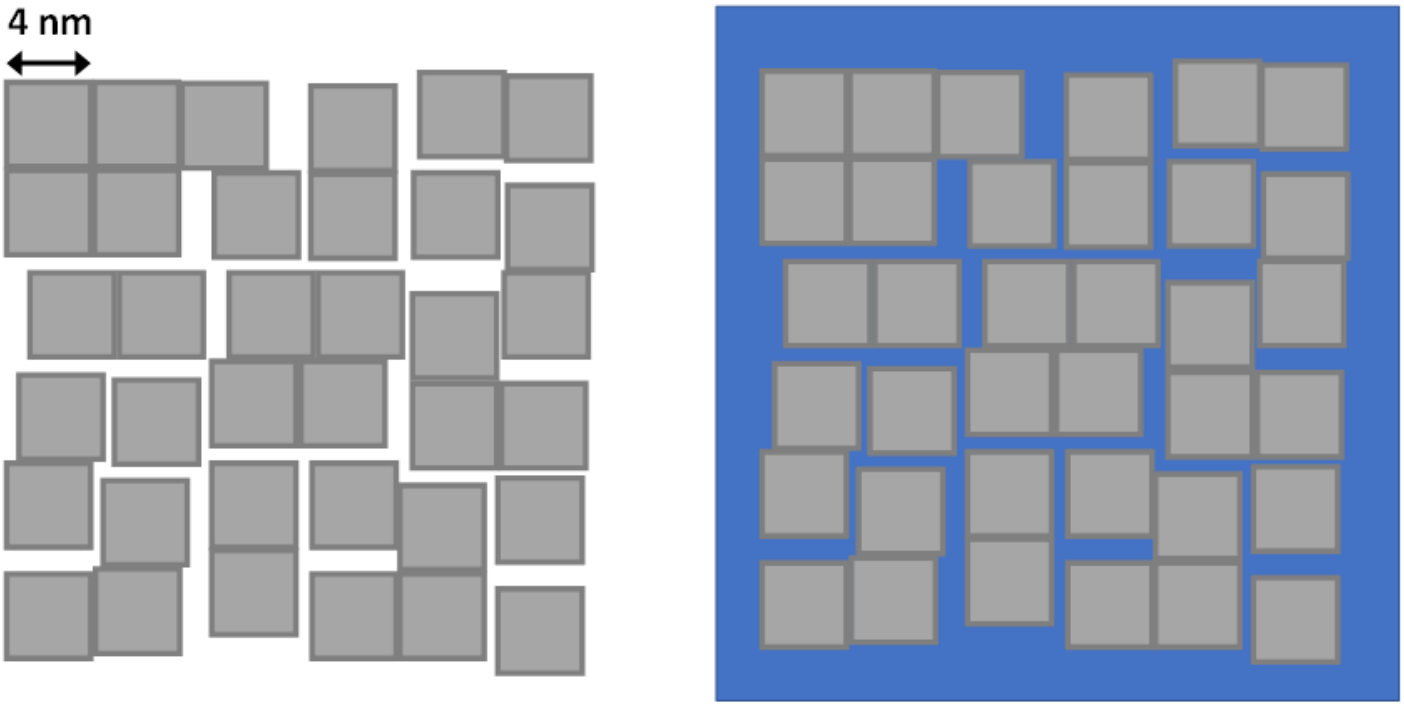

Figure 10

An idealized illustration of a cross-section of a fibril aggregate composed of 6-by-6 fibrils, each with a width of 4 nanometres. Left: dry state with imperfect packing of cellulose fibrils, right: water swollen state with imperfections in the cellulose fibril packing remaining. The aggregation pattern of cellulose fibrils may vary along the length direction of a fibril aggregate. The length direction is perpendicular to the plane of the illustrated cross-section (not shown).

Supplementary Files

This is a list of supplementary files associated with this preprint. Click to download.

- PTLarssonSI20210527.docx